INDIAN JOURNAL OF SCIENCE AND TECHNOLOGY

RESEARCH ARTICLE

Impact of Bi_2O_3 on the Structural, Optical, Radiation Shielding, and Dielectric Analysis of Lead Borosilicate Glasses Doped with TiO_2

Madabushanam Gopi Krishna[1], Ravi Kumar Guntu[2]*, N Rama Krishna Chand[3], Md Shareefuddin[1], N V Prasad[1]*

1 Department of Physics, Osmania University, Hyderabad, 500 007, Telangana, India
2 Department of Physics, Sreenidhi Institute of Science and Technology, JNT University, Hyderabad, 501 301, Telangana, India
3 Department of Physics, Andhra Loyola College, Krishna University, Vijayawada, 520 008, AP, India

OPEN ACCESS

Received: 16-01-2024
Accepted: 22-02-2024
Published: 30-05-2024

Citation: Krishna MG, Guntu RK, Chand NRK, Shareefuddin M, Prasad NV (2024) Impact of Bi_2O_3 on the Structural, Optical, Radiation Shielding, and Dielectric Analysis of Lead Borosilicate Glasses Doped with TiO_2. Indian Journal of Science and Technology 17(22): 2305-2315. https://doi.org/10.17485/IJST/v17i22.114

* **Corresponding authors**.

drgrk1985@gmail.com

nvp1969@gmail.com

Funding: None

Competing Interests: None

Published By Indian Society for Education and Environment (iSee)

ISSN
Print: 0974-6846
Electronic: 0974-5645

Abstract

Objective: The principal aim of this investigation was to assess the impact of bismuth oxide on the optical properties, radiation shielding characteristics, and dielectric behavior of lead borosilicate glasses doped with titanium oxide at a low concentration. **Method:** We intended to utilize the conventional rapid melt quenching method to produce glasses with the following chemical composition: 25 PbO+ 15 B_2O_3 + 0.1 TiO_2 + (59.9-x) SiO_2 : x Bi_2O_3($0 \leq x \leq 12$). **Findings:** XRD and SEM analyses were used to confirm the samples' non-crystalline properties, while DTA investigations were used to evaluate the samples' ability to form glass. The numerous structural elements were identified through the utilization of FT–IR and Raman analyses. The optical characteristics of glasses are determined by optical absorption studies. The findings derived from optical absorption spectral analyses revealed a progressive increase in the concentration of octahedral Ti^{4+} ions with the mol% Bi_2O_3 concentration. In order to analyse the glasses' dielectric properties, an impudence analyser was employed. The results obtained from these inquiries indicate that glasses do contain Bi_2O_3 at concentrations lower than 12 mol% experience a progressive increase in dielectric constant values. Further investigation is conducted into the radiation shielding properties of the glasses. **Novelty:** The findings indicate that the values of the glasses' optical band gap, radiation shielding ability, dielectric constant, and thermal stability are all directly correlated with their Bi_2O_3 concentration.

Keywords: FTIR; Raman; OBG; MAC; Activation Energy

1 Introduction

Borosilicate glasses, which have higher ionic conductivity, a higher glass transition temperature, and greater chemical stability than pure borate and phosphate glasses, are a prime example of the mixed glass network formation effect[1]. These improved qualities enable the application of these glasses in batteries, sealants, and bone replacement materials. The presence of BPO_4 structural units in addition to BO_3 and BO_4 units makes borophosphate glasses structurally captivating[2]. The silicate tetrahedral units SiO_4 with charge compensation are physically linked to the tetrahedral boron units $[BO_{4/2}]$ in the unique structure of the BPO_4 units. Previous research on these glasses concluded that their greater glass transition temperature, chemical endurance, and stability were caused by the SiO_4 units present in them[3]. The PbO addition improves these glasses' ionic conductivity and chemical resistance even further. Promising possibilities for enhanced solid electrolytes in electrochemical cells were these glasses. Energy storage is becoming a more pressing issue due to the fast-growing number of battery-powered products such as computers, mobile phones, medical equipment, cars, and more. To keep up with this demand, safer, more energy-dense, and smaller batteries are needed[4]. The greatest options for the needs of energy storage are rapid ion conducting glasses, such as lead borosilicate glasses, which represent a substantial category of solid electrolytes[5]. Bismuth oxide is a heavy metal oxide that is mostly utilized in glasses as a refining agent and as a catalyst for polymerization. Thanks to their many unique qualities, including strange thermal expansion, aberrant UV transmission, and low softening temperature, borosilicate glasses are more popular than traditional silicate glasses and offer several advantages[6]. The majority of transition metal ions have multivalent states, and the composition of the material may affect how stable they are in glassy materials. Depending on their valence and coordination states in the glass matrix, they can either increase or diminish the capacity to produce glass[7]. According to earlier research on transition metal ion-doped glasses, titanium ions mostly exist in the divalent state, are most stable in the absence of oxidation and reduction and occupy octahedral positions due to their moderating function within the glass network[8]. Since Ti^{4+}ions are luminous activators that create laser emission in the UV, visible, and near-infrared wavelength range, the TiO_2-doped bismuth lead borosilicate glasses are very important in the field of telecommunication[9]. Investigation into bismuth lead borosilicate glasses doped with Ti^{4+} ions seems to be the most beneficial, cumulative, academic, and technological area of interest. The production of enclosed fastening of metallic glass materials and glass planar photosensitive waveguides was significantly improved using Ti^{4+} ions doped bismuth lead borosilicate glasses[10]. We are focusing on the impact of Ti^{4+} valence states on bismuth lead borosilicate glasses in this study by examining various structural characteristics (IR and Raman investigations), optical characteristics, radiation shielding, and dielectric characteristics.

2 Methodology

Experimental

For this investigation, the chemical composition of 25 PbO+ 15 B_2O_3 + 0.1 TiO_2 + (59.9-x) SiO_2 : x Bi_2O_3 has been selected. Table 1 contains the complete composition. The precise concentrations of the analytic grades of PbO, Bi_2O_3, Boric acid (H_3BO_3), SiO_2, and TiO_2 chemicals (all expressed in mole percent) were carefully mixed in an agate mortar and then liquefied in a densely walled crucible in an automatic temperature furnace for about 40 minutes, or until a transparent liquid without of voids created.

Table 1. Chemical composition of 25 PbO+ 15 B_2O_3 + 0.1 TiO_2 + (59.9-x) SiO_2 : x Bi_2O_3 glass materials

Glass	PbO (mol%)	B_2O_3 (mol%)	TiO_2 (mol%)	SiO_2 (mol%)	Bi_2O_3 (mol%)
TiBi-0	25	15	0.1	59.9	0
TiBi-3	25	15	0.1	56.9	3
TiBi-5	25	15	0.1	54.9	5
TiBi-8	25	15	0.1	51.9	8
TiBi-10	25	15	0.1	49.9	10
TiBi-12	25	15	0.1	47.9	12

The final mixture was poured into a brass mold, which was subsequently annealed gradually at 240 degrees Celsius in a muffle furnace. Utilizing a Scale Tech digital weighing balance, the mass of the prepared containers was measured with a precision of 10^{-4} grams. The O-xylene liquid and the Archimedes method were employed to determine the densities ($\pm$ 0.0001 g/cm^3) of the glass samples that were produced. After reducing the samples to the specified dimensions of 1x 1 x 0.2 cm^3, they were appropriately polished. To validate the non-crystalline characteristics of the fabricated glasses, X-ray diffraction (XRD) traces were captured utilizing a PAN analytical instrument equipped with X'Pert^3 Powder. Sample surface morphology as captured by

the Hitachi S-3700N Spectrometer. The DTG – 60H (SHIMADZU) was utilized to conduct differential thermal analysis (DTA) on the prepared samples. The instrument operated at a heating rate of 5.0 °C per minute, covering a temperature range of 27 to 1400 °C. The produced glasses were subjected to optical absorption (OA) investigations at room temperature using an Agilent Technologies Carry 5000 UV to NIR Region instrument with a 0.1 nm resolution within the 200–2200 nm wavelength range. The spectral measurements in the FT-IR range of 400–4000 cm^{-1} were acquired using a Perkin Elmer Spectrum Two instrument with four scans. Raman spectral measurements were acquired utilizing a Horrible Jobin Yvon Germany, LASER (633 nm), 20-2000 nm instrument, 100x objective lens. Utilizing Phy-x and PSD software to obtain radiation shielding measurements. The auto lab impudence analyzer was utilized to conduct dielectric measurements across a frequency range of 1 kHz to 1 MHz.

3 Results and Discussion

The developed glasses of 25 PbO+ 15 B_2O_3 + 0.1 TiO_2 + (59.9-x) SiO_2 : x Bi_2O_3 are photographed in Figure 1**(a)**. Figure 1**(b)** shows the X-ray diffraction patterns of the test glasses, which shows that the X-ray diffraction measurements have no crystalline peaks. The TiBi-12 glass was found to have the highest diffraction intensities about XRD intensities. Previous studies have suggested that the tightest structural compactness, smallest atomic distance, highest density, and least molar volume could be responsible for the highest diffraction intensities of test samples. Using energy dispersion spectra, the chemical makeup of the test sample consisting of 25 PbO+ 15 B_2O_3 + 0.1 TiO_2 + (59.9-x) SiO_2 : x Bi_2O_3 was confirmed. which denotes the substances found in the test glasses, including silicon, oxygen, bismuth, lead, titanium, and boron. This view shows the chemical analysis of one of the TiBi-12 test glasses, as shown in Figure 1 **(c)**. which shows the following atomic weight percentages: 25 mol% PbO, 15 mol% B_2O_3, 0.1 mol% TiO_2, 47.9 mol% SiO_2, and 12 mol% Bi_2O_3. The 25 PbO+ 15 B_2O_3 + 0.1 TiO_2 + (59.9-x) SiO_2 : x Bi_2O_3 test samples' surface morphology was noted, which are observed to have no crystalline behavior. Morphological reports of the test TiBi-12 glass is shown in Figure 2 and suggests glassy behavior at 10, 20, 50, and 100 micro meter range[11].

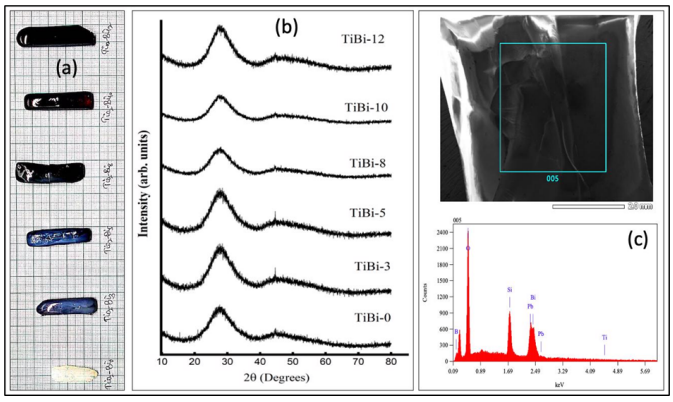

Fig 1. (a) The photograph, (b) XRD patterns and (c) chemical analysis of the TiBi-12 glass of 25 PbO+ 15 B_2O_3 + 0.1 TiO_2 + (59.9-x) SiO_2 : x Bi_2O_3 glasses

The physical properties of 25 PbO+ 15 B_2O_3 + 0.1 TiO_2 + (59.9-x) SiO_2 : x Bi_2O_3 glasses reported in Table 2. For the prepared glasses, as the concentration of TiO_2 increases, the density depends and an increase in average molecular weight is observed. As the concentration of TiO_2 increases, the anticipated ionic concentration, field strength, and molar volume increase whereas the associated ionic radius and polaron radius decrease[12].

Fig 2. Surface morphology of the TiBi-12 glass at 20, 50 and 100 mm range

Table 2. Physical properties of 25 PbO+ 15 B_2O_3 + 0.1 TiO_2 + (59.9-x) SiO_2 : x Bi_2O_3 glasses measures at room temperature

Glass	TiBi-0	TBi-3	TiBi-5	TiBi-8	TiBi-10	TiBi-12
ρ (gm/cm^3)	4.163	4.533	4.756	4.972	5.288	5.408
N_i (x10^{20})	-	2.08	2.32	2.39	2.44	2.49
r_i (Å)	-	0.169	0.165	0.163	0.16	0.159
r_p (Å)	-	6.8	6.55	6.49	6.44	6.4
V_m (cm^{3}mol^{-1})	30.27	27.10	26.36	25.77	25.25	22.17
F_i (x10^{14}cm^{-2})	-	2.16	2.33	2.37	2.41	2.44

It was discovered that the glass transition temperature (T_g) of the 25 PbO+ 15 B_2O_3 + 0.1 TiO_2+ (59.9-x) SiO_2 : x Bi_2O_3 glasses was 420 °C, and that the value of T_g increased as the concentration of Bi_2O_3 increased. The value of the exothermic peak, which is seen at the glass crystallization temperature (T_c) of roughly 850 °C, rises with the concentration of Bi_2O_3 [13]. The thermal stability of glass was assessed using T_g and T_c and is provided in Table 3.

Table 3. Summary on data of DTA studies of 25 PbO+ 15 B_2O_3 + 0.1 TiO_2 + (59.9-x) SiO_2 : x Bi_2O_3 glasses

Glass	TiBi-0	TBi-3	TiBi-5	TiBi-8	TiBi-10	TiBi-12
T_g (°C)	591	592	595	596	599	601
Thermal stability	0.735	0.737	0.740	0.744	0.748	0.752

The usual vibrational bands of borate groups, silicate groups, PbO, Bi_2O_3, and TiO_2 structural units are displayed in the FT-IR spectra of 25 PbO+ 15 B_2O_3 + 0.1 TiO_2+ (59.9-x) SiO_2 : x Bi_2O_3 glasses, as provided in Table and illustrated in Figure 4. SiO_2 vibrational modes, including asymmetrical and symmetrical Si-O-Si units, are observed at around 1029–1003 cm^{-1} and 768–789 cm^{-1}. Regions of 1413–1394 cm^{-1}, 924–940 cm^{-1}and 854-867 cm^{-1} respectively, are the bands that originate from BO_3, BO_4 units, and Bi–O connections. The Pb–O units were observed at 521-540 cm^{-1} in the vicinity, respectively. Within the range of 721–742 cm^{-1}, the bands resulting from Ti–O specific vibrations will be predicted [14,15].

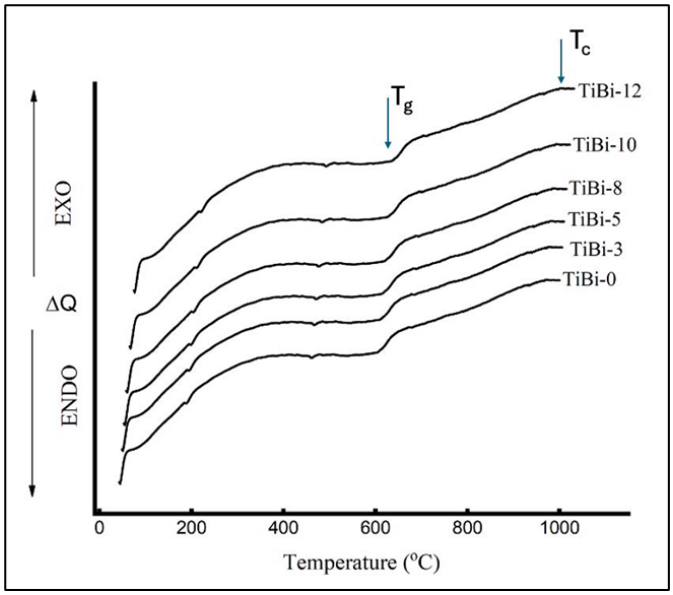

Fig 3. DTA thermograms of the 25 PbO+ 15 B_2O_3 + 0.1 TiO_2 + (59.9-x) SiO_2 : x Bi_2O_3 glasses

As seen in Figure 5, the Raman spectra of the 25 PbO+ 15 B_2O_3 + 0.1 TiO_2 + (59.9-x) SiO_2 : x Bi_2O_3 glasses exhibit characteristic vibrational bands of PbO, Bi_2O_3, TiO_2, silicate groups, and borate groups. Table 5 contained the Raman band assignment. The SiO_2 vibrational modes observed at 784 – 799 cm^{-1} and 1052 – 1067 cm^{-1} include Si-O-Si bending and stretching units.

The regions 794 –780 cm^{-1}, 755 – 770 cm^{-1} and 677 – 689 cm^{-1} are home to the bands that originate from BO_3, BO_4 units, and B-O connections, respectively. The Pb–O symmetric units were observed at 667 and 690 cm^{-1} in the vicinity, respectively.

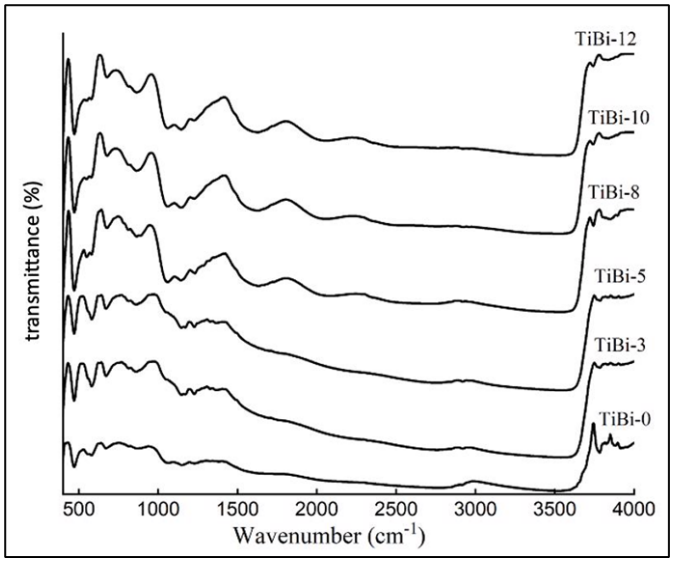

Fig 4. FT-IR spectra of 25 PbO+ 15 B_2O_3 + 0.1 TiO_2 + (59.9-x) SiO_2 : x Bi_2O_3 glasses recorded at room temperature

Table 4. Data on infrared spectra of 25 PbO+ 15 B_2O_3 + 0.1 TiO_2 + (59.9-x) SiO_2 : x Bi_2O_3 glasses recorded at room temperature

Glass	TiBi-0	TBi-3	TiBi-5	TiBi-8	TiBi-10	TiBi-12
BO_3 units (cm^{-1})	1413	1409	1406	1401	1398	1394
Si-O-Si asymmetrical (cm^{-1})	1029	1023	1018	1014	1008	1003
Si-O-Si symmetrical (cm^{-1})	768	772	777	782	785	789
BO_4 units (cm^{-1})	924	926	929	933	936	940
Pb-O units (cm^{-1})	521	523	528	530	535	540
Bi-O linkages (cm^{-1})	855	857	859	862	865	867
Ti-O vibrations (cm^{-1})	721	724	729	735	739	742

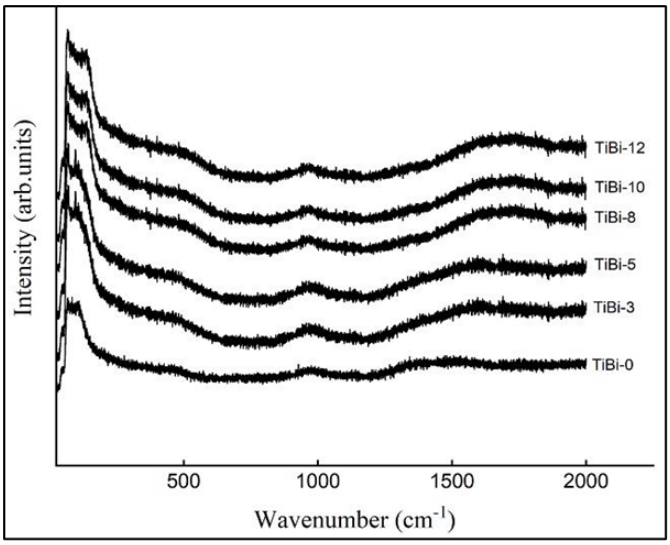

Fig 5. Raman spectra of 25 PbO+ 15 B_2O_3 + 0.1 TiO_2 + (59.9-x) SiO_2 : x Bi_2O_3 glasses recorded at room temperature

The areas 606 – 612 cm^{-1} are where the Bi-O vibrations were seen. In the range of 911 – 937 cm^{-1}, the bands resulting from TiO_2 specific vibrations are anticipated [16,17].

Table 5. Summary on Raman spectra of 25 PbO+ 15 B_2O_3 + 0.1 TiO_2 + (59.9-x) SiO_2 : x Bi_2O_3 glasses

Glass	TiBi-0	TBi-3	TiBi-5	TiBi-8	TiBi-10	TiBi-12
BO_3 units (cm^{-1})	794	791	788	785	783	780
Si-O-Si bending units (cm^{-1})	795	798	800	803	805	808
Si-O-Si stretching units (cm^{-1})	1059	1062	1065	1067	1070	1072
BO_4 units (cm^{-1})	755	758	761	763	767	770
Pb-O units (cm^{-1})	677	676	679	677	686	689
Bi-O linkages (cm^{-1})	399	403	406	408	413	416
Ti-O specific vibrations (cm^{-1})	911	917	923	928	933	937

Figure 6(**a**) displays the optical absorption spectra of glasses containing 25 PbO+ 15 B_2O_3 + 0.1 TiO_2 + (59.9-x) SiO_2 : x Bi_2O_3 that were recorded at room temperature. By looking at the glasses' Tauc plots, as seen in Figure 6 (**b**), one can determine the band gap values of glasses. The glass in this image was found to have the highest TiO_2 concentration (12 mol%) out of all the other glasses. The outcomes of the current glasses, along with the identifications and assessments of the absorption spectra, are shown in Table 6 [18]. The Tauc plots and measured optical absorption spectra of the present glasses indicate that the optical band gap parameter decreases with increasing Bi_2O_3 content. This is due to an increase in non-bridging oxygens (NBOs) and bond defects in the network of glass ceramics, which causes Ti^{4+} and Bi^{3+} ions to depolymerize the network. The addition of Bi_2O_3 to the glass network up to a concentration of 12 mol% causes the TiO_6 ions to rise and other donor ions to form, which have a tendency to overlap with excited states of electrons. These numerous theories show that the impurity energy band diffuses into the original band gap, causing the optical band gap to diminish [19].

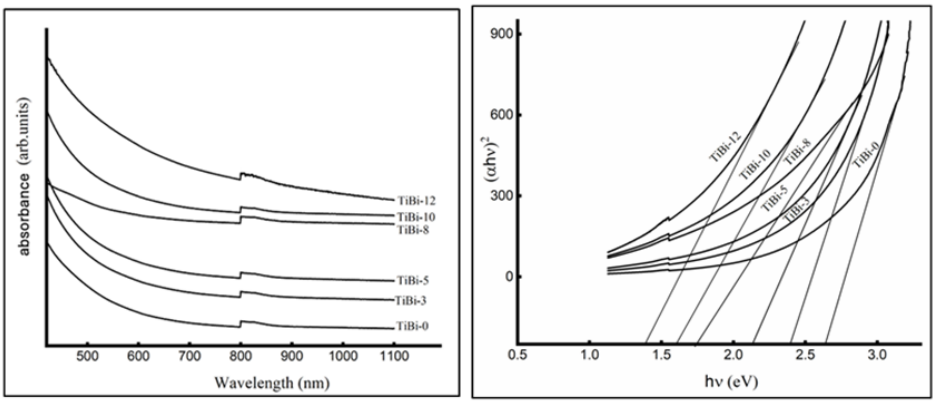

Fig 6. (a) Optical absorption spectra of 25 PbO+ 15 B_2O_3 + 0.1 TiO_2 + (59.9-x) SiO_2 : x Bi_2O_3 glasses recorded at room temperature, (b) Tauc plots of 25 PbO+ 15 B_2O_3 + 0.1 TiO_2 + (59.9-x) SiO_2 : x Bi_2O_3 glasses

At low Bi_2O_3 concentrations, Ti^{4+} ions deform and occupy octahedral positions, according to the optical absorption spectra of the 25 PbO+ 15 B_2O_3 + 0.1 TiO_2 + (59.9-x) SiO_2 : x Bi_2O_3 glasses. Although the occupancy rate increases with concentration up to 12 mol%, the octahedral occupancy in the glass matrix decreases with concentration. An increment of 12 mol% of Bi_2O_3 in the concentration of Bi^{3+} ions at octahedral sites within the glass system leads to an increased generation of bound electrons at donor centers and NBOs. As such, excited states of localized electrons initially contained in Ti^{3+} sites correspond with unoccupied third- state configurations of neighboring Ti^{4+} ion sites. Consequently, the absorption edge shifts to the higher wavelength area, and the optical band gap shrinks dramatically due to the broadening and merging of the impurity band with the main band. The observed modifications in the absorption edge and optical band gap may be attributed to a reduction in the interaction between the p-electrons in the conductions band of silicate ions and the localized d electrons of substitutionally positioned titanium ions. Therefore, the octahedral titanium ions act as network modifiers, reducing the stiffness of the generated materials. Bi_2O_3 concentrations greater than 12 mol% in the glasses cause a decrease in both the

concentration of NBOs and the density of related groups that contain ions positioned interstitially. This may indicate a decrease in the quantity of electrons occupying donor centers. The increase of the optical band gap causes an intrinsic shift in favor of shorter wavelengths at the absorption edge.

Table 6. Summary on optical absorption of 25 PbO+ 15 B_2O_3 + 0.1 TiO_2 + (59.9-x) SiO_2 : x Bi_2O_3 glass materials recorded at room temperature

Glass	TiBi-0	TBi-3	TiBi-5	TiBi-8	TiBi-10	TiBi-12
Optical band gap (eV)	2.6	2.4	2.2	1.7	1.6	1.4
Urbach Energy (eV)	0.0835	0.0831	0.0829	0.0826	0.0821	0.0816

The shielding properties of 25 PbO+ 15 B_2O_3 + 0.1 TiO_2 + (59.9-x) SiO_2 : x Bi_2O_3 glasses are investigated using the Phy-X/PSD program. The half value layer describes the radiation's ability to pass through the test glasses. It also aids in shielding design. The mean free path of the sample shows how well photons can go through it. It's found that the variation in photon energy in the MAC values is increasing[20]. Based on the data, the K-absorption edge at roughly 0.0679 MeV indicates the presence of Ti^{4+} ions. Figure 7**(a), (b), (c),** and **(d)** show how MAC, MFP (mean free path), HVL (half layer width), and RPE (radiation protection efficiency) change when incident photon energy increases. Because of the TiO_6 octahedral units, test glasses are denser. The structural units of Pb-O-Si, Bi-O-B, and Bi-O-Ti are the additional cause of the high glass density. An exponential decaying pattern can be used to illustrate the MAC tendency versus photon energy.

Additionally, as the content of Bi_2O_3 in the glass samples increased, the MAC values were also shown to increase. For the glasses recorded as TiBi-0 to TiBi-12 the MAC values at low energy photons E = 0.015 MeV are 17.181 and 17.371, respectively. Based on the amount of Bi_2O_3 contained in the glasses, the minimal variation in the MAC values of the test glass can be understood. The other two molecular components of the glass system, such as Bi_2O_3, PbO and B_2O_3, are maintained at an equimolar fraction in each of the manufactured glasses. The mol% of Bi_2O_3 in these glasses is increased from 0.0 to 12 mol% compared to the Bi_2O_3 concentration.

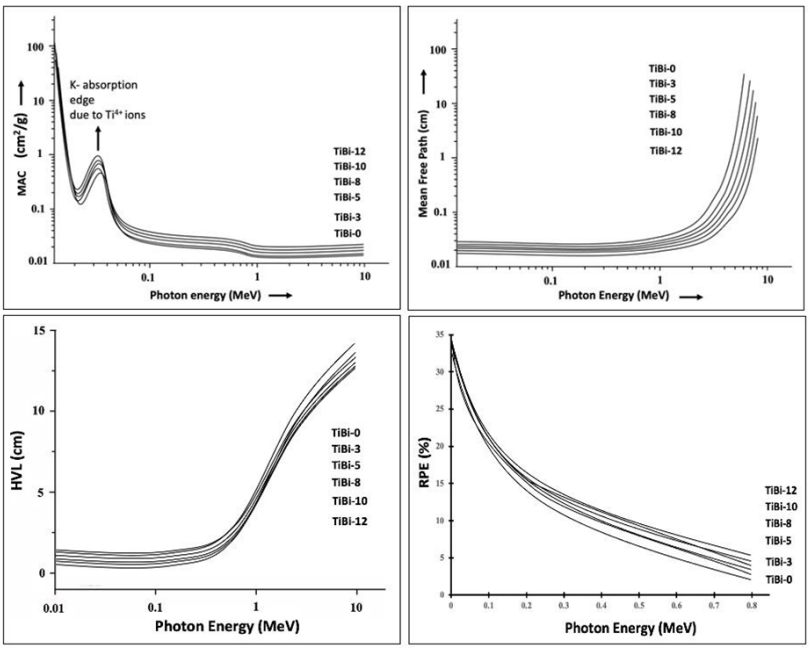

Fig 7. (a) Variation in MAC, (b) Variation in MFP, (c) Variation in HVL, and (d) Variation in RPE with Photon energy of 25 PbO+ 15 B_2O_3 + 0.1 TiO_2 + (59.9-x) SiO_2 : x Bi_2O_3 glasses

The NBOs during glass formation are another factor contributing to the shift in MAC values with increasing Bi^{3+} ions. Due to the site symmetry of the Pb^{2+}, Bi^{3+}, Si^{4+}, and Ti^{4+} ions in the glasses, the MAC values increase more in the low photon energy region. LAC has values of 0.17 to 0.2 cm^{-1} at an energy of 1 MeV for glasses TiBi-0.0 to TiBi-2.5, respectively. Glass TiBi-12 has the greatest LAC values due to its maximum atomic number and ρ [21]. Additionally, the figure shows that at these selected

Table 7. Summary on radiation shielding properties of 25 PbO+ 15 B_2O_3 + 0.1 TiO_2 + (59.9-x) SiO_2 : x Bi_2O_3 glasses recorded at room temperature

Glass	TiBi-0	TBi-3	TiBi-5	TiBi-8	TiBi-10	TiBi-12
MAC (at 0.02 MeV) cm^2/g	68	75	83.7	87	91.5	106
MFP (at 10 MeV) cm	59.71	52.75	35.6	10.11	8.27	7.26
HVL (at 10 MeV) cm	14.85	14.51	13.92	13.42	12.91	12.53
RPE (%)	32.71	33.03	33.64	33.95	34.12	34.63

energies, the Bi_2O_3 concentration has a linear effect on the LAC. This could also be explained by the previously indicated spectrum of metals (e.g., Bi_2O_3) and non-metals (e.g., PbO, B_2O_3, SiO_2, and TiO_2) present in the glass combinations. From the same angle, the other dependent metrics, such as MFP, HVL, and RPE, also rise in proportion to the concentration of Bi^{3+} ions in the test glasses. TiBi-12 glass was discovered to have good values for MAC, MFP, HVL, and RPE; TiBi-0, TiBi-3, TiBi-5, TiBi-8, and TiBi-12 glasses will also be advantageous as shielding glasses[22]. Generally, the only variables influencing the test glasses' radiation protection effectiveness and shielding phenomena are the concentration of Bi_2O_3 and their thickness.

At 1 kHz, 10 kHz, and 100 kHz frequencies, as well as in the temperature range of 30 °C to 250 °C, the dielectric characteristics of the 25 PbO + 15 B_2O_3 + 0.1 TiO_2 + (59.9-x) SiO_2 : x Bi_2O_3 glasses are measured. Wherein the dielectric constant, dielectric loss, ac conductivity, activation energy conduction, and temperature area of relaxation have all been evaluated. The best results were observed with the TiBi-12 glass. Figure 8 illustrates how the dielectric constant changes with temperature. The variation in the dielectric constant of TiBi-12 glass for frequency ranges of 1 kHz, 10 kHz, and 100 kHz is depicted in the inset of the same image. The temperature-dependent variation in di-electric loss is seen in Figure 9. The fluctuation in the dielectric loss of the TiBi-12 glass at 1 kHz, 10 kHz, and 100 kHz frequency ranges is reported in the inset of the same figure. The response of AC conductivity to an inverse temperature variation is shown in Figure 10. The inset of the same figure reports the change in A.E. with increasing Bi_2O_3 concentration. Due to variations in space charge polarization, the dielectric constant, dielectric loss, ac conductivity, temperature zone of relaxation, and activation energy conduction with temperature and frequency all change as the concentration of Bi_2O_3 increases. Polarization, which causes the fluctuations in the values of dielectric constant, dielectric loss, ac conductivity, temperature area of relaxation, and activation energy conduction with temperature and frequency.

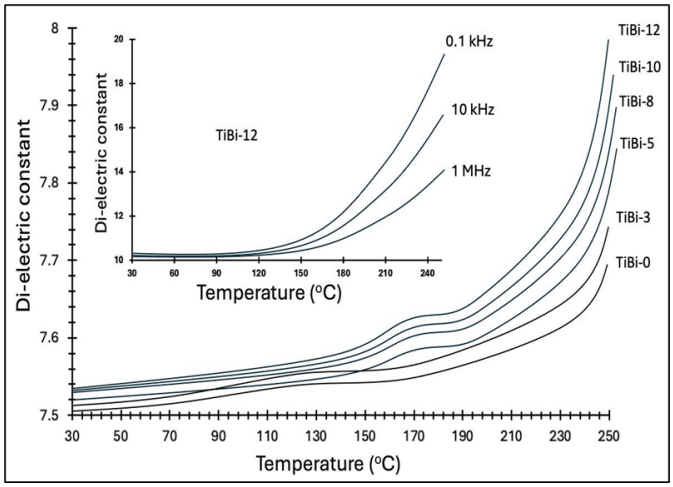

Fig 8. The variation in dielectric constant of 25 PbO+ 15 B_2O_3 + 0.1 TiO_2 + (59.9-x) SiO_2 : x Bi_2O_3 glasses with temperature. Inset shows the variation of dielectric constant of glass TiBi-12 with temperature at different frequencies

Space charge polarization is the result of some of the charge carriers in the glass network trapping other charge carriers inside the material's boundaries when they move across short atomic distances at lower frequencies. This movement distorts the local field, raising the capacitance and ultimately the dielectric constant[23]. Bi_2O_3 enhances the space charge polarization, dielectric constant, loss tangent, and AC conductivity of the host glasses at concentrations as high as 12 mol%. In addition, a reversal trend in the Bi_2O_3 concentration is observed at 12 mol%. As the concentration of Bi_2O_3 rises, the relaxation time shift shows compositional dependence. As the concentration of Bi_2O_3 in the host glass rises over 12 mol%, the cross-linking of Bi^{3+} tetrahedral ions decreases. By lowering the production of polaron-lattice ion couplings, dipoles' ac conductivity, loss tangent,

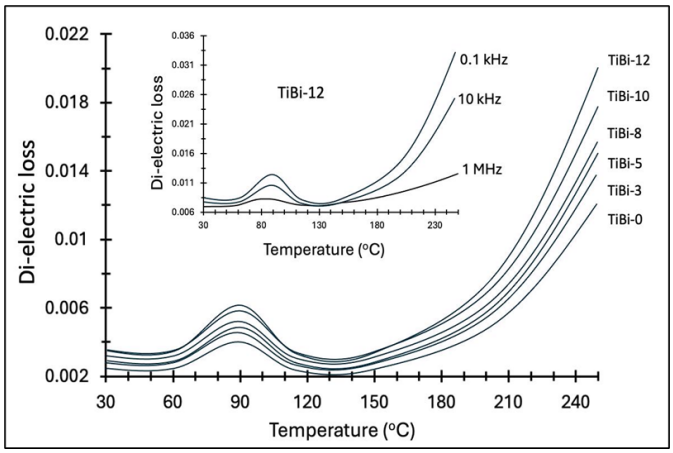

Fig 9. The variation of dielectric loss of 25 PbO+ 15 B_2O_3 + 0.1 TiO_2 + (59.9-x) SiO_2 : x Bi_2O_3 glasses with temperature. Inset shows the variation of dielectric loss with temperature at different frequencies of glass TiBi-12

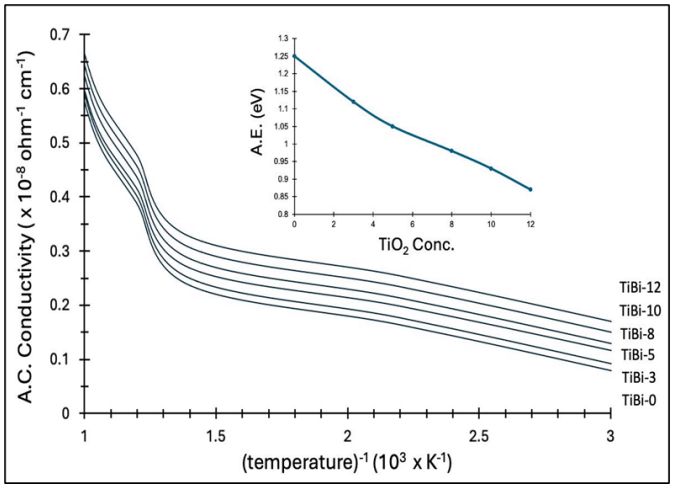

Fig 10. Variation of AC Conductivity of 25 PbO+ 15 B_2O_3 + 0.1 TiO_2 + (59.9-x) SiO_2 : x Bi_2O_3 glasses with 1/T. Inset shows the variation of activation energy with concentration of Bi_2O_3

Table 8. Summary on dielectric properties of 25 PbO+ 15 B_2O_3 + 0.1 TiO_2 + (59.9-x) SiO_2 : x Bi_2O_3 glasses

Glass	TiBi-0	TBi-3	TiBi-5	TiBi-8	TiBi-10	TiBi-12
Di electric constant at 250°C, 1KHz	7.69	7.74	7.83	7.88	7.95	7.98
Di electric loss at 250°C, 1KHz	0.0125	0.013	0.0139	0.0145	0.018	0.019
Ac Conductivity at 300K (s_{ac}) (ohm^{-1} cm^{-1}) (x 10^{-8})	5.31	6.75	7.82	8.71	9.25	10.16
Temp region of relaxation (°C)	71-98	73-99	76-104	79-109	81-112	83-116
A.E for conduction (eV)	1.25	1.12	1.05	0.98	0.93	0.87

and dielectric constant are all improved. The activation energy of the glasses rises by more than 12 mol% of the Bi_2O_3 content when seen from the same angle. One of the polarization mechanisms in materials that causes the dielectric constant and AC conductivity to increase with temperature is space charge polarization, at a particular frequency. Changing ions (octahedrally positioned titanium and borate ions combined with Pb^{2+} ions) can induce bonding issues in the glass network. Space charge polarization is triggered as a result of charge carriers being able to travel through these flaws more readily. At all frequencies and temperatures, there is a positive association between the activation energy and the dielectric properties and a progressive increase in concentration up to 12 mol%. This implies that an increase in space charge polarization is caused by the growing amounts of octahedral Ti^{4+} ions acting as modifiers. Tetrahedral Ti^{4+} ions expand when Bi_2O_3 concentration rises over 12 mol% because they create glass connections with other tetrahedral glass network members. In the end, this expansion leads to a decrease in the polarization of the space charge. The QMT model infers that the density states of defects at the Fermi level $N(E_f)$ determine the AC conductivity at lower frequencies. It is found that an increase in TiO_2 concentration (up to 12 mol%) results in an increase in AC conductivity. This implies that the glass network or localized defect energy levels have more free charge carriers available for conduction. Nonetheless, a reversal in conductivity is noted above 12 mol% TiO_2. As modifications, Ti^{4+} ions occupying octahedral locations in the glass network will enhance by up to 12 mol% of TiO_2 the concentration of dangling bonds produced by lead ions and Ti^{4+} ions with different cations in the existing glass samples[24,25]. The primary factors contributing to the improved structural, optical, radiation shielding, and dielectric properties of current glasses are the atomic radius of Ti^{4+} ions, their trivalent oxidation state, the density of the glasses, the intermolecular force between the Ti^{4+} ions and Bi^{3+}, Pb^{2+}, Si^{4+} and B^{3+} ions, the number of non-bridging oxygens within the glasses, and the octahedral tendency of Ti^{4+} ions within the glasses. The specific results such as thermal stability (0.752), optical band gap (1.4 eV), radiation protection ability (~ 34.63 %) and dielectric constant (~7.98) of present glasses are noticed to be great and comparable with previous literature (cited reference 14, 18, 20 and 24) are suggestible as thermally stable, optically active, radiation shielding dielectric glass resource.

4 Conclusion

The results of the radiation shielding, optical, structural, and dielectric analyses of the glasses 25 PbO+ 15 B_2O_3 + 0.1 TiO_2 + (59.9-x) SiO_2 : x Bi_2O_3 lead to the following conclusions: Glassy behavior is demonstrated by studies on glasses that use SEM and XRD. The EDX analysis shows the chemical composition along with the proportion of atomic weight. Physical characteristics including density (~ 5.408 gm/cm^3) and molar volume (~ 22.17 cm^3 mol^{-1}) were discovered to be optimal for the TiBi-12 glass. In the DTA analyses of glasses, it was also found that the TiBi-12 glass had the highest values of GTT (approximately 594 °C) and thermal stabilities (~ 0.752). The FT-IR and Raman analyses give an assessment of the structural changes in the glass network caused by compositional variances. The optical absorption measurements further show that the optical band gap (1.4 eV) values are exclusively reliant on the concentration of Bi_2O_3 at very low concentrations. Radiation shielding properties like MAC (~106 cm^2/g) and RPE (~34.63 %) demonstrate that Bi^{3+} ions are the only source of dependence for the shielding behavior. The dielectric properties of the glasses show the range of their dielectric constant (~7.98), dielectric loss (~ 0.019), ac conductivity (~ 10.16 x 10^{-8} ohm^{-1} cm^{-1}) and A.E. (~ 0.87 eV) values. These results further show that the dielectric behavior of the glasses depends only on the presence of Bi^{3+} ions. All things considered, the 25 PbO+ 15 B_2O_3 + 0.1 TiO_2 + (59.9-x) SiO_2 : x Bi_2O_3 glasses that were produced are beneficial glass materials that are mechanically hard, optically active, dielectric, and radiation-shielding.

Author's contribution statement

Mr. Madabushanam Gopi Krishna: Methodology, characterization, results, analysis and report drafting, Dr. Ravi Kumar Guntu: Methodology, results, analysis, and report correction, Dr. N. Rama Krishna Chand: Results and analysis, Dr. Md Shareefuddin: suggestions and report corrections, Dr. NV Prasad: Supervision, suggestions, and report corrections.

Acknowledgement

The authors thank the management of Sreenidhi Institute of Science and Technology, for their needful help and moral support during overall completion of the investigation.

References

1) Pisarski WA, Kowalska K, Kuwik M, Pisarska J, Dorosz D, Kochanowicz M, et al. Enhanced mid-IR luminescence of Er3+ ions at 2.7 μm in TiO2-GeO2-BaO-Ga2O3 glasses. *Journal of Luminescence*. 2024;265. Available from: https://dx.doi.org/10.1016/j.jlumin.2023.120227.

2) Hamad MK, Sayyed MI, Mhareb MHA, Sadeq MS, Dwaikat N, Almessiere MA, et al. Effects of TiO2, V2O5, MnO2 and Tl2O3 on structural, physical, optical and ionizing radiation shielding properties of strontium boro-tellurite glass: An experimental study. *Optical Materials*. 2022;127. Available from: https://dx.doi.org/10.1016/j.optmat.2022.112350.
3) Fong WL, Bashar K, Baki SO, Karim MKA, Sayyed MI, Mahdi MA, et al. Influence of Bi2O3 content on structural, optical and radiation shielding properties of transparent Bi2O3-Na2O-TiO2-ZnO-TeO2 glass ceramics. *Radiation Physics and Chemistry*. 2022;200:110289–110289. Available from: https://dx.doi.org/10.1016/j.radphyschem.2022.110289. doi:10.1016/j.radphyschem.2022.110289.
4) Karami H, Zanganeh V, Ahmadi M. Study nuclear radiation shielding, mechanical and Acoustical properties of TeO2-Na2O-BaO-TiO2 alloyed glasses. *Radiation Physics and Chemistry*. 2023;208. Available from: https://dx.doi.org/10.1016/j.radphyschem.2023.110917.
5) Mahdy EA, Sahbal KM, Mabrouk M, Beherei HH, and YKAM. Enhancement of glass-ceramic performance by TiO2 doping: In vitro cell viability, proliferation, and differentiation. *Ceramics International*. 2021;47(5):6251–6261. Available from: https://doi.org/10.1016/j.ceramint.2020.10.203.
6) Wang Z, Xu R. Effects of TiO2 on the structural characteristics of CaO–SiO2–Al2O3–TiO2 glass in the same superheat state studied by Raman spectra. *Ceramics International*. 2023;49(16):26494–26504. Available from: https://dx.doi.org/10.1016/j.ceramint.2023.05.184.
7) He P, Luo Z, Liang H, Liu X, Tong J, Zhou Z, et al. Study on the structure and optical properties of the Tb3+-doped SrO–MgO–SiO2–TiO2–B2O3 glasses. *Optical Materials*. 2023;144. Available from: https://doi.org/10.1016/j.optmat.2023.114349.
8) Deng L, Fu Z, Mingxing Z, Li H, Yao B, He J, et al. Crystallization, structure, and properties of TiO2-ZrO2 co-doped MgO-B2O3-Al2O3-SiO2 glass-ceramics. *Journal of Non-Crystalline Solids*. 2022;575. Available from: https://dx.doi.org/10.1016/j.jnoncrysol.2021.121217.
9) Li Y, Fu Z, Zheng K, Wang J, Sun X. Effect of TiO2 addition amount on BaO–CaO–Al2O3 -SiO2 glass-bonded Al2O3 ceramics. *Ceramics International*. 2023;49(15):25261–25268. Available from: https://dx.doi.org/10.1016/j.ceramint.2023.05.060.
10) Herrera A, Londoño F, Balzaretti NM. Structural and optical properties of Nd3+ doped GeO2-PbO glass modified by TiO2 for applications in laser and fiber amplifier. *Optical Materials*. 2021;113. Available from: https://dx.doi.org/10.1016/j.optmat.2021.110884.
11) Shankar J, Kumar AS, Raju P, Anjaiah J, Ali SM, Rani GN, et al. Synthesis, microstructure and ferroelectric properties of PbO-TiO2-B2O3 based glass ceramics. *Materials Today: Proceedings*. 2022;64(Part 1):585–589. Available from: https://dx.doi.org/10.1016/j.matpr.2022.05.120.
12) Jia H, Zhan L, Han L, Zhang X, Xie J, Li H, et al. Effects of TiO2 content and crystallization treatments on elastic modulus of alkali-free aluminosilicate glass. *Journal of Solid State Chemistry*. 2023;325. Available from: https://dx.doi.org/10.1016/j.jssc.2023.124177.
13) Alencar MVS, Bezerra GVP, Silva LD, Schneider JF, Pascual MJ, Cabral AA. Structure, Glass Stability and Crystallization Activation Energy of SrO-CaO-B2O3-SiO2 glasses doped with TiO2. *Journal of Non-Crystalline Solids*. 2021;554. Available from: https://dx.doi.org/10.1016/j.jnoncrysol.2020.120605.
14) Richter LJ, Beckmann CM, Ihlemann J. UV laser generated micro structured black surface on commercial TiO2-containing glass. *Applied Surface Science*. 2022;601. Available from: https://dx.doi.org/10.1016/j.apsusc.2022.154231.
15) Zalapa-Garibay MA, Reyes-López SY. Effect of NiO, ZrO2 and TiO2 on the formation of glass-ceramic cordierite in the MgO–Al2O3–SiO2–MoO3 system. *Journal of Materials Research and Technology*. 2024;28:3805–3824. Available from: https://dx.doi.org/10.1016/j.jmrt.2023.12.176.
16) Fong WL, Bashar KA, Baki SO, Karim MKA, Sayyed MI, Mahdi MA, et al. Influence of Bi2O3 content on structural, optical and radiation shielding properties of transparent Bi2O3-Na2O-TiO2-ZnO-TeO2 glass ceramics. *Radiation Physics and Chemistry*. 2022;200. Available from: https://dx.doi.org/10.1016/j.radphyschem.2022.110289.
17) Wang Y, Zhang X, Zhang J, Wang Z. Controllable synthesis of SrO-B2O3-SiO2-TiO2 glass-ceramics: Insight into the crystallization kinetics and dielectric properties. *Materials Chemistry and Physics*. 2023;296. Available from: https://dx.doi.org/10.1016/j.matchemphys.2022.127273.
18) Chen P, Cheng C, Li T, Wang Y, Wang C, Zhang L. Significantly improved dielectric properties of TiO2 ceramics through acceptor-doping and Ar/H2 annealing. *Ceramics International*. 2021;47(2):1551–1557. Available from: https://dx.doi.org/10.1016/j.ceramint.2020.08.268.
19) Wang Z, Zhao Y, Zhang C. Comparative investigation on the structure and physical properties of CeO2/TiO2/Sb2O3-doped bismuth borosilicate glasses. *Journal of Non-Crystalline Solids*. 2020;544. Available from: https://dx.doi.org/10.1016/j.jnoncrysol.2020.120190.
20) Zandona A, Patzig C, Rüdinger B, Hochrein O, Deubener J. TiO2(B) nanocrystals in Ti-doped lithium aluminosilicate glasses. *Journal of Non-Crystalline Solids: X*. 2019;2(2):1–9. Available from: https://dx.doi.org/10.1016/j.nocx.2019.100025.
21) Li H, Yin Z, Deng L, Wang S, Fu Z, Ma Y. Effect of SiO2/Al2O3 ratio on the structure and electrical properties of MgO–Al2O3–SiO2 glass-ceramics doped with TiO2. *Materials Chemistry and Physics*. 2020;256. Available from: https://dx.doi.org/10.1016/j.matchemphys.2020.123653.
22) El-Khayatt AM, Saudi HA, AlRowis NH. Synthesis and Characterization of Zinc-Lead-Phosphate Glasses Doped with Europium for Radiation Shielding. *Sustainability*. 2023;15(12):1–21. Available from: https://dx.doi.org/10.3390/su15129245.
23) Es-soufi H, Ouachouo L, Mahmoud KG, Sayyed MI, Essoussi H, Bih L. Effect of Bi2O3 on the Structural, Mechanical, and Radiation Gamma Shielding Properties of the Boro-Silica-Phosphate Glasses. *Silicon*. 2023;15(16):6945–6961. Available from: https://dx.doi.org/10.1007/s12633-023-02549-6.
24) Ramanujan CS, Alrowaili ZA, Sekhar KC, Alzahrani JS, Shareefuddin M, Haritha L, et al. Synthesis and Optimization of Bi2O3-B2O3-Cr2O3 Glass System for Structural, Optical, and Radiation Shielding Properties. *Journal of Electronic Materials*. 2023;52(10):6445–6459. Available from: https://dx.doi.org/10.1007/s11664-023-10613-5.
25) Alzahrani JS, Kavas T, Kurtulus R, Olarinoye IO, Al-Buriahi MS. Physical, structural, mechanical, and radiation shielding properties of the PbO–B2O3–Bi2O3–ZnO glass system. *Journal of Materials Science: Materials in Electronics*. 2021;32(14):18994–19009. Available from: https://dx.doi.org/10.1007/s10854-021-06414-3.